Theory of homogeneous vapour condensation and surface deposition from boundary layers

M. D. Camejo[1] **and L. L. Bonilla**[1,2]*

[1] G. Millán Institute of Fluid Dynamics, Nanoscience and Industrial Mathematics,
Universidad Carlos III de Madrid, 28911 Leganés, Spain

[2] School of Engineering and Applied Sciences. Harvard University, 29 Oxford Street, Cambridge,
MA 02138, USA

* Email address for correspondence: bonilla@ing.uc3m.es

Homogeneous condensation of vapours mixed with a carrier gas in the stagnation point boundary layer flow near a cold wall is considered. There is a condensation region near the wall with supersaturated vapour. Assuming that the surface tension times the molecular area is much larger than the thermal energy far from the wall, droplets are nucleated exclusively in a narrow nucleation layer where the Zeldovich flux of clusters surpassing the critical nucleus size is at a maximum. The vapour condenses in the free molecular regime on the droplets, which are thermophoretically attracted to the wall. Unlike the narrow condensation region for heterogeneous condensation on solid particles, in the case of homogeneous condensation the condensation region is wide even when the rate of vapour scavenging by droplets is large. A singular perturbation theory of homogeneous vapour condensation in boundary layer flow approximates very well the vapour and droplet density profiles, the nucleation layer and the deposition rates at the wall for wide ranges of the wall temperature and the scavenging parameter B. A key point in the theory is to select a trial vapour number density profile among a one parameter family of profiles between an upper and a lower bound. The maximum of the Zeldovich flux for supercritical nuclei provides the approximate location of the nucleation layer and an approximate droplet density profile. Then the condensate number of molecules and the vapour density profile are calculated by matched asymptotic expansions that also yield the deposition rates. For sufficiently large wall temperatures, a more precise corrected asymptotic theory is given.

Key words: boundary layer structure, condensation/evaporation, multiphase flows

1. Introduction

The effects of condensation in fluid flows have been studied in many situations of interest ranging from condensation trail formation in aircraft wakes (Paoli, Helie & Poinsot 2004), shock-tube experiments (Luo *et al.* 2007), steam turbines (Delale & Crighton 1998) and combustion chambers (Rosner 2000). When there are solid particles in the carrier gas, the supersaturated vapours condense on them and they are carried to cold walls thermophoretically (Gökoglu & Rosner 1986; Castillo & Rosner 1988, 1989; Neu, Bonilla & Carpio 2009). This heterogeneous condensation

is important in aerosol formation (Davis 1983; Friedlander 2000; Peeters, Luijten & van Dongen 2001), fouling and corrosion in biofuel plants (Pyykönen & Jokiniemi 2003), outside vapour deposition processes used for making optical fibres (Filippov 2003; Tandon & Murtagh 2005), chemical vapour deposition, vapour condensation and aerosol capture by cold plates or rejection by hot ones (Rosner 2000).

In this paper, we consider homogeneous condensation of vapours mixed with a carrier gas in the stagnation point boundary layer flow near a cold wall. Gökoglu & Rosner (1986), Castillo & Rosner (1988, 1989), Filippov (2003) and Neu *et al.* (2009) considered heterogeneous condensation in the case of diluted vapours in a carrier gas and a diluted suspension of solid particles upon which the vapour may condense. Castillo & Rosner (1988, 1989) study a simple thermophysical model in which the carrier gas is considered to be incompressible, the Soret and Dufour effects are ignored and the particles and droplets move towards the wall by thermophoresis (Davis 1983; Zheng 2002). Gökoglu & Rosner (1986) and Filippov (2003) deal with more complicated thermophysical models in which the carrier gas is compressible, its viscosity has an algebraic dependence on temperature and the Soret effect is included. In all cases, the presence of vapours and suspended solid particles does not affect the laminar boundary layer flow of the carrier gas, which is described by coupled ordinary differential equations in a similarity variable. In this paper, we adapt the thermophysical model by Castillo & Rosner (1988, 1989) to the case of homogeneous condensation. The carrier gas does not contain solid particles and therefore droplets formed as clusters of condensate molecules surpass the critical nucleus size. These droplets are created at the Zeldovich flux as described in Wu (1997) and grow in the free molecular regime. Under different experimental conditions, there are other nucleation rates that improve the classical nucleation theory (Nowakowski & Ruckenstein 1991; Sinha, Wyslouzil & Wilemski 2009) and there are other growth laws that hold for any droplet size (Sinha *et al.* 2009). It is straightforward to extend our analysis using these nucleation and growth rates instead of the Zeldovich flux and the free-molecular-regime growth law.

The numerical solutions of the model equations for the Hiemenz stagnation point flow are interpreted using a singular perturbation approach based on the fact that thermal energy is small compared to surface tension times molecular area and that the scavenging rate at which vapour condenses on droplets is large. Under these conditions, droplets of condensate are created in a narrow nucleation layer about the point x_M where the Zeldovich flux is at a maximum. The location of this point is unknown because it depends on the droplet density that has to be calculated as part of the problem. There is a wider condensation layer that may extend to the wall in which vapour is supersaturated and condenses on existing droplets. We find x_M from a trial vapour number density that optimizes the maximum number density of the condensate vapour, and then we approximate the droplet density and the number of condensate molecules for $0 \leqslant x \leqslant x_M$ by using matched asymptotic expansions and obtain the vapour number density $c(x)$ and the deposition rates at the wall.

The rest of the paper is organized as follows. Section 2 describes the model. In § 3, the equations and boundary conditions of the model are written for the simple case of a Hiemenz stagnation point flow. In § 4, we obtain upper and lower bounds of the vapour density profile. The numerical solution of the thermophysical model equations is described in § 5. Section 6 contains a description of our singular perturbation approach. Lastly § 7 contains our conclusions.

2. Model

Consider a dilute vapour of number density $\tilde{c}(\tilde{\boldsymbol{x}})$ in a carrier gas. The mass fraction of vapour is sufficiently small with respect to the mass fraction of the carrier gas that the velocity and temperature fields (assumed to be stationary) $\tilde{\boldsymbol{u}}(\tilde{\boldsymbol{x}})$ and $\tilde{T}(\tilde{\boldsymbol{x}})$ are not affected by the condensation and deposition processes. The vapour will condense in droplets after a homogeneous nucleation process. Let $\tilde{\rho}(\tilde{\boldsymbol{x}})$ be the number density of droplets and let $\tilde{n}(\tilde{\boldsymbol{x}})$ be the the number of condensed vapour molecules equal to the volume of a droplet divided by the molecular volume of the condensed vapour. Then $\tilde{\rho}(\tilde{\boldsymbol{x}})\tilde{n}(\tilde{\boldsymbol{x}})$ is the number density of the condensate. New droplets are generated by homogeneous condensation of vapour at a rate given by the stationary Zeldovich flux of clusters surpassing the size of a critical nucleus n_* to become droplets; see (1.19) of Wu (1997). Thus the droplet density in a laminar flow varies according to

$$\tilde{\nabla} \cdot \left[\left(\tilde{\boldsymbol{u}} - \alpha \nu \frac{\tilde{\nabla}\tilde{T}}{\tilde{T}} \right) \tilde{\rho} \right] = \sqrt{\frac{2\tilde{v}^2\tilde{\sigma}}{\pi\tilde{m}_v}} \tilde{c}^2 \left(1 + n_*^{-1/3}\right)^2 \left(1 + n_*^{-1}\right)^{1/2} \mathrm{e}^{-(\sigma^3/2\eta^2)} H(\tilde{c} - \tilde{c}_e), \quad (2.1)$$

$$\eta = \ln\left(\frac{\tilde{c}}{\tilde{c}_e}\right), \quad (2.2)$$

$$\sigma = \frac{2\tilde{\sigma}}{k_B\tilde{T}} \left(\frac{4}{3}\pi\tilde{v}^2\right)^{1/3}, \quad (2.3)$$

$$n_* = \left(\frac{\sigma}{\eta}\right)^3. \quad (2.4)$$

Here $\tilde{m}_v$, $\tilde{v}$ and $\tilde{\sigma}$ are the molecular mass, the molecular volume and the surface tension of the vapour, respectively; k_B, $\tilde{T}(\boldsymbol{x})$, η, σ and n_* are the Boltzmann constant, the temperature, the supersaturation, the non-dimensional surface tension and the critical nucleus size, respectively. In (2.1), the velocity of droplets equals the flow velocity plus the thermophoretic velocity $-\alpha\nu\tilde{\nabla}\ln\tilde{T}$, where ν is the kinematic viscosity of the carrier gas and the dimensionless thermophoretic coefficient α that depends on the droplet radius but will be considered here to be constant for simplicity. Droplets are produced only in supersaturated regions where the vapour density $\tilde{c}(\boldsymbol{x})$ is larger than its equilibrium value $\tilde{c}_e$, which is enforced by the Heaviside function $H(\tilde{c} - \tilde{c}_e)$ on the right-hand side of (2.1). We shall assume that the carrier gas is incompressible. This leads to simpler equations and asymptotic expressions (Neu *et al.* 2009) but it also overestimates the particle deposition rates; see Filippov (2003) for the case of heterogeneous condensation. For wall temperatures larger than $\tilde{T}_\infty/2$ this effect is not too large, and our asymptotic theory is applicable to more realistic models including compressibility of the carrier gas. For an incompressible carrier gas, $\tilde{\nabla}\cdot\tilde{\boldsymbol{u}} = 0$ and (2.1) becomes

$$\left(\tilde{\boldsymbol{u}} - \alpha\nu\frac{\tilde{\nabla}\tilde{T}}{\tilde{T}}\right) \cdot \tilde{\nabla}\tilde{\rho} = \alpha\nu\tilde{\rho}\tilde{\nabla}\cdot\frac{\tilde{\nabla}\tilde{T}}{\tilde{T}} + \sqrt{\frac{2\tilde{v}^2\tilde{\sigma}}{\pi\tilde{m}_v}}\tilde{c}^2\left(1 + n_*^{-1/3}\right)^2$$

$$\times \left(1 + n_*^{-1}\right)^{1/2} \mathrm{e}^{-\sigma^3/(2\eta^2)} H(\tilde{c} - \tilde{c}_e). \quad (2.5)$$

Once the droplets are created, vapour condenses on them in supersaturation regions thereby increasing their size. In this work we have adopted the simple thermophysical model described by Castillo & Rosner (1988) and applied it to the case of Na$_2$SO$_4$ vapours diluted in air with a mean free path of 0.34 microns at a temperature of

3

1400 K (Neu *et al.* 2009). A cluster of 400 molecules of Na_2SO_4 (the critical size for a supersaturation of 0.35 and a wall temperature of 1200 K) has a diameter of ~ 1 nm. This yields a Knudsen number of 340, much larger than 1. Hence the basic hypothesis of a free molecular condensation regime is applicable. Then the droplets, which grow from the nucleus size (which can be ignored), are much smaller than the mean free path, and therefore in a stationary flow we have (Castillo & Rosner 1988; Filippov 2003)

$$\left(\tilde{\boldsymbol{u}} - \alpha \nu \frac{\tilde{\boldsymbol{\nabla}} \tilde{T}}{\tilde{T}} \right) \cdot \tilde{\boldsymbol{\nabla}} \tilde{n} = (\tilde{c} - \tilde{c}_e) \sqrt{\frac{k_B \tilde{T}}{2 \pi \tilde{m}_v}} \, (36 \pi \tilde{v}^2)^{1/3} \, \tilde{n}^{2/3} H(\tilde{c} - \tilde{c}_e) \, H(\tilde{n} - n_*). \quad (2.6)$$

Both droplet nucleation and growth feed from the supersaturated vapour, and therefore these processes acts as sinks in the balance equation for the vapour number density:

$$(\tilde{\boldsymbol{u}} \cdot \tilde{\boldsymbol{\nabla}} - D \tilde{\Delta}) \tilde{c} = - \sqrt{\frac{k_B \tilde{T}_\infty}{\tilde{m}_v}} \left(\frac{6 v^4}{\pi} \right)^{1/6} \left[\sqrt{\frac{3 \tilde{T}}{\tilde{T}_\infty}} (\tilde{c} - \tilde{c}_e) \tilde{\rho} \tilde{n}^{2/3} H(\tilde{n} - n_*) \right.$$

$$\left. + \sqrt{\frac{\sigma_\infty}{2 \pi}} n_* \tilde{c}^2 \left(1 + n_*^{-1/3} \right)^2 \left(1 + n_*^{-1} \right)^{1/2} e^{-(\sigma^3 / 2 \eta^2)} \right] H(\tilde{c} - \tilde{c}_e). \, (2.7)$$

Here we have converted the Zeldovich flux of number of droplets per unit time in number density per unit time multiplying the right-hand side of (2.1) by the critical nucleus n_*. Likewise the number of molecules per droplet and per unit time on the right-hand side of (2.6) has been multiplied by $\tilde{\rho}$ to appear on the right-hand side of (2.7) as number density of vapour molecules per unit time adsorbed by droplets as they grow. In (2.7), we have defined a temperature-independent dimensionless surface tension $\sigma_\infty = 2 \tilde{\sigma} \left(4 \pi \tilde{v}^2 / 3 \right)^{1/3} / (k_B \tilde{T}_\infty)$, where $\tilde{T}_\infty$ is a constant reference temperature, for example far from the wall. We have $\sigma = \sigma_\infty \tilde{T}_\infty / \tilde{T}$ and the dimensionless surface tension in the Zeldovich exponential is inversely proportional to the temperature. In (2.7), the vapour follows the carrier gas flow and we neglect the Soret effect (Castillo & Rosner 1988; Neu *et al.* 2009). The solution of more detailed models (for example in outside vapour deposition, OVD) show that changes due to the Soret effect are relatively small (Filippov 2003; see also García Ybarra & Castillo 1997 for the case in which the Soret effect plays an important role).

In (2.5)–(2.7), the equilibrium number density $\tilde{c}_e$ is given by the Clausius–Clapeyron relation which, for the case of an incompressible carrier gas, is

$$\frac{\tilde{c}_e}{\tilde{c}_\infty} = \frac{\tilde{T}_d}{\tilde{T}} \exp \left[\left(\frac{\tilde{\Lambda}_K}{k_B \tilde{T}_d} - \frac{\tilde{\Lambda}_K}{k_B \tilde{T}} \right) \right], \quad (2.8)$$

$$\tilde{\Lambda}_K = \tilde{\Lambda} - 2 \tilde{\sigma} \left(\frac{4 \pi \tilde{v}^2}{3 \tilde{n}} \right)^{1/3}, \qquad \frac{\tilde{\Lambda}_K}{k_B \tilde{T}_\infty} = \frac{\tilde{\Lambda}}{k_B \tilde{T}_\infty} - \frac{\sigma_\infty}{\tilde{n}^{1/3}}. \quad (2.9)$$

Here $\tilde{c}_\infty$ is the vapour number density far from the wall, $\tilde{\Lambda}$ is the heat of vapourization and $\tilde{T}_d$ is the dew point temperature at which $\tilde{c}_\infty = \tilde{c}_e$ in the absence of flow. $\tilde{\Lambda}_K$ given by (2.9) contains the correction due to the finite size of the droplets (Kelvin effect) which is quite small even for the size of the critical nucleus n_*. Since n is usually much larger than n_*, we shall ignore the Kelvin effect, $\tilde{\Lambda}_K \approx \tilde{\Lambda}$ and, to be consistent,

we shall also ignore the correction factor $(1 + n_*^{-1/3})^2 (1 + n_*^{-1})^{1/2}$ in (2.1), (2.5) and (2.7).

In the presence of flow, the dew point temperature changes, and part of the problem we have to solve is to determine its shift. If we have vapour density $\tilde{c}_\infty$ and temperature $\tilde{T}_\infty > \tilde{T}_d$ far from the wall, and lower the temperature locally below $\tilde{T}_d$, the vapour becomes supersaturated there. Hence nucleation becomes possible and the production of nuclei for further condensation is initiated. In the stationary flow we consider, the temperature satisfies the equation

$$\tilde{\boldsymbol{u}} \cdot \tilde{\boldsymbol{\nabla}} \tilde{T} = \kappa\, \tilde{\Delta} \tilde{T}, \qquad (2.10)$$

where κ is the constant thermal diffusivity. In this equation, we have ignored the Dufour effect and also the effect of the latent heat of condensation because the vapour mass fraction is very small compared to that of the carrier gas. We will not specify here the equation for the velocity of the carrier gas because our theory can be used for different flow fields.

The boundary conditions for our problem are

$$\tilde{T} = \tilde{T}_\infty, \quad \tilde{c} = \tilde{c}_\infty, \quad \tilde{\rho} = 0, \quad \tilde{n} = 0 \quad \text{at infinity (far from the wall),} \qquad (2.11)$$
$$\tilde{T} = \tilde{T}_w, \quad \tilde{c} = \tilde{c}_e(\tilde{T}_w) \quad \text{at the wall.} \qquad (2.12)$$

We consider $\tilde{T}_w < \tilde{T}_d < \tilde{T}_\infty$. Since the wall temperature is below the dew point, the vapour will condense on the cold wall, where it will be in local equilibrium with the liquid coating it. Thus $\tilde{c} = \tilde{c}_e$ at the wall. At infinity, the vapour density is $\tilde{c}_\infty$. At some distance from the wall, there is an interface Γ (the dew surface) between the nucleation–condensation region, where some vapour molecules condense forming droplets and some other molecules condense on the created droplets, and an outer region at a higher temperature where there is no vapour condensation. Locating Γ is part of the problem. On Γ, $\tilde{c}_* = \tilde{c}_e(\tilde{T}_*)$ (from now on, the asterisk will identify magnitudes on the interface), and the normal derivative of $\tilde{c}$ is continuous. Note that the dew point temperature at Γ will be different from the dew point temperature in the absence of flow, $\tilde{T}_d$. We have

$$\tilde{T} = \tilde{T}_*, \quad \tilde{c}_* = \tilde{c}_e(\tilde{T}_*), \quad \boldsymbol{n} \cdot \tilde{\boldsymbol{\nabla}} \tilde{c}|_{\Gamma-} = \boldsymbol{n} \cdot \tilde{\boldsymbol{\nabla}} \tilde{c}|_{\Gamma+}, \quad \tilde{\rho} = 0, \quad \tilde{n} = n_* \quad \text{at } \Gamma. \quad (2.13)$$

Assuming that we have calculated the carrier gas velocity field, $\tilde{\boldsymbol{u}}(\tilde{\boldsymbol{x}})$, in principle we have enough boundary conditions to determine $\tilde{T}$, $\tilde{c}$, $\tilde{\rho}$, $\tilde{n}$ and Γ.

(i) We solve the elliptic equation (2.10) for $\tilde{T}$ with one condition at infinity and another at the wall.

(ii) For a given location of Γ, the first-order equations (2.5) and (2.6) for $\tilde{\rho}$ and $\tilde{n}$ in the condensation region have one boundary condition each at Γ. The elliptic equation (2.7) has Dirichlet boundary conditions (2.11) at infinity and $\tilde{c}_* = \tilde{c}_e(\tilde{T}_*)$ at Γ. Similarly, the solution of (2.7) for $\tilde{c}$ in the condensation region satisfies (2.12) at the wall and $\tilde{c}_* = \tilde{c}_e(\tilde{T}_*)$ at Γ.

(iii) Given an arbitrary location of Γ, the two elliptic problems for $\tilde{c}$ are solved inside and outside the condensation region. Then the location of Γ is changed until the additional condition (2.13) – that the normal derivative of $\tilde{c}$ is continuous at Γ – is satisfied. This determines the position of the dew point interface.

Note that the vapour density $\tilde{c}_*$ at the interface is smaller than $\tilde{c}_\infty$ because the condensation region is a vapour sink and the diffusion causes a vapour density deficit
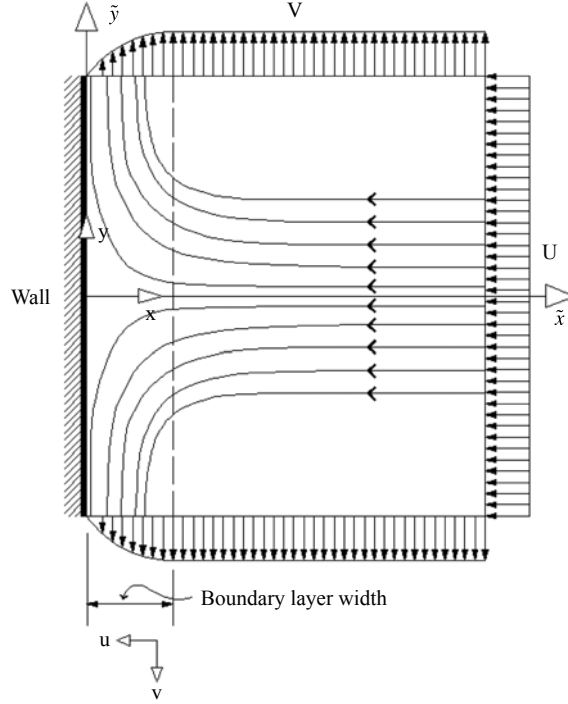
FIGURE 1. Sketch of plane stagnation-point flow.

even in the dry region. Since $\tilde{c}_* = \tilde{c}_e(\tilde{T}_*)$ and $\tilde{c}_\infty = \tilde{c}_e(\tilde{T}_d)$, we have $\tilde{c}_e(\tilde{T}_*) < \tilde{c}_e(\tilde{T}_d)$. As $\tilde{c}_e(\tilde{T})$ is an increasing function, we obtain $\tilde{T}_* < \tilde{T}_d$; due to the flow, the temperature at the interface Γ is lower than the dew point temperature in the absence of flow $\tilde{T}_d$.

3. Hiemenz planar stagnation-point flow

We consider as an example the Hiemenz stagnation-point flow in the half-space $\tilde{x} > 0$ depicted in figure 1 (Schlichting & Gersten 2000). There is a solid wall at $\tilde{x} = 0$ and the $\tilde{x}$-velocity of the incoming flow is asymptotic to $-\tilde{x}/\tau$ with a given strain rate τ^{-1}. The boundary layer thickness is $l_b = \sqrt{\nu\tau}$, which we shall adopt as the unit of length. Then the unit of velocity is $\nu/l_b = \sqrt{\nu/\tau}$. We shall adopt $\tilde{c}_\infty$ as the unit of $\tilde{c}$ and of $\tilde{\rho}$, and $\tilde{T}_\infty$ as the unit of temperature. Their values are given in table 1. Since $\tilde{n}$ is dimensionless, we set $n(x) = \tilde{n}(l_b x)$.

The dimensionless x component of the velocity is a function of x, denoted by $-u(x)$, $u > 0$, whereas the dimensionless y component of the velocity is $u'(x)y$. (Here and in the rest of the paper, $f'(x)$ means $\mathrm{d}f/\mathrm{d}x$.) Hence $u(x)$ is the parameter-free solution of the well-known Hiemenz boundary value problem (BVP) of stagnation in plane flow Schlichting & Gersten (2000):

$$u''' + u\,u'' + 1 - u'^2 = 0, \quad x > 0, \tag{3.1}$$

$$u(0) = u'(0) = 0, \quad u'(+\infty) = 1. \tag{3.2}$$

In non-dimensional units, (2.10) becomes

$$T'' + P_r u T' = 0, \quad x > 0, \tag{3.3}$$

$\tilde{T}_\infty$ (K)	$\tilde{T}_d$ (K)	$[c] = [\rho] = \tilde{c}_\infty$ (cm^{-3})	$[n]$ (–)	l_b (mm)	v/l_b (cm s^{-1})	D (cm^2 s^{-1})	$\tilde{v}$ (cm^3)	$\tilde{m}_v$ (g)	$\tilde{\sigma}$ (J m^{-2})
1713	1400	1.9×10^{13}	1	6.26	0.24	0.083	8.87×10^{-23}	2.358×10^{-22}	0.05

TABLE 1. Typical parameters for homogeneous condensation of Na_2SO_4 in air (Castillo & Rosner 1988).

to be solved with the boundary conditions

$$T(0) = T_w = \tilde{T}_w / \tilde{T}_\infty, \quad T(+\infty) = 1, \tag{3.4}$$

where $P_r = \nu/\kappa$ is the Prandtl number (which is 0.7 for air). Equations (2.5)–(2.9) with the boundary conditions (2.11)–(2.13) become

$$U\rho' + \alpha \left(\frac{T'}{T}\right)' \rho = -\frac{Bc^2}{S_c \sqrt{6\pi\epsilon}} \exp\left(-\frac{1}{2\eta^2 T^3 \epsilon^3}\right) H(c - c_e), \quad x > 0, \tag{3.5}$$

$$\rho(+\infty) = 0, \tag{3.6}$$

$$U = u + \alpha \frac{T'}{T}, \tag{3.7}$$

$$c_e(x) = \frac{T_d}{T(x)} \exp\left[\frac{\Lambda}{\epsilon}\left(\frac{1}{T_d} - \frac{1}{T(x)}\right)\right], \tag{3.8}$$

$$Un' = -\frac{B}{S_c}(c - c_e) T^{1/2} n^{2/3} H(n - n_*) H(c - c_e), \quad x > 0, \tag{3.9}$$

$$n(+\infty) = 0, \tag{3.10}$$

$$n_* = \left(\frac{1}{\epsilon\eta T}\right)^3, \tag{3.11}$$

$$c'' + S_c u c' = B\left[\frac{\epsilon^{-7/2} c^2}{\sqrt{6\pi}\eta^3 T^3} e^{-(1/2\eta^2 T^3 \epsilon^3)} + (c - c_e)\rho T^{1/2} n^{2/3} H(n - n_*)\right] H(c - c_e), \tag{3.12}$$

$$c(0) = c_e(0), \quad c(+\infty) = 1, \tag{3.13}$$

where

$$\left.\begin{aligned} S_c = \frac{\nu}{D}, \quad \epsilon = \frac{k_B \tilde{T}_\infty}{2\tilde{\sigma}\left(\frac{4\pi}{3}\tilde{v}^2\right)^{1/3}}, \quad \frac{\Lambda}{\epsilon} = \frac{\tilde{\Lambda}}{k_B \tilde{T}_\infty}, \\ B = \frac{(3\tilde{v})^{2/3} \tilde{c}_\infty l_b^2}{D}\left(\frac{2}{\pi}\right)^{1/6}\sqrt{\frac{k_B \tilde{T}_\infty}{\tilde{m}_v}}. \end{aligned}\right\} \tag{3.14}$$

Representative values for the dimensionless parameters of the problem are indicated in table 2 for Na_2SO_4 vapour in air as in Castillo & Rosner (1988). $S_c = \nu/D$ is the Schmidt number, and $\epsilon/\Lambda \ll 1$ measures how fast $c_e(x)$ decays as $x < x_*$ moves away from the dew point location x_*. In fact, from (3.8) we find

$$\frac{c_e(x)}{c_*} = \frac{T_*}{T(x)} \exp\left(\Lambda \frac{T(x) - T_*}{\epsilon T_* T(x)}\right) \approx \exp\left(-\frac{x_* - x}{\delta_e}\right), \tag{3.15}$$

and

$$\delta_e = \frac{\epsilon T_*^2}{\Lambda T'_*} \tag{3.16}$$

is the dimensionless decay length of $c_e(x)$ (Neu *et al.* 2009). The inverse dimensionless surface tension $1/\sigma_\infty = \epsilon$ is small and therefore the Zeldovich flux on the right-hand side of (3.5) has a sharp maximum and it decays very rapidly to zero
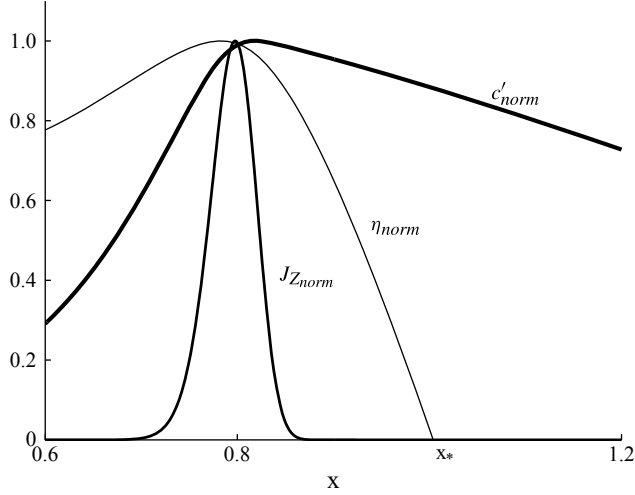
FIGURE 2. c', η and J_Z for $\tilde{T}_w = 1000$ K. The three curves have been normalized so that their maxima always equal 1.

	α	$\frac{\epsilon}{\Lambda}$	P_r	S_c	ϵ	B
I	0.1	0.0515	0.7	1.8	0.0644	1.09×10^4
II	0.1	0.0515	0.7	1.8	0.0644	1.63×10^5

TABLE 2. Dimensionless parameters for I, $l_b = 6.26$ mm, and II, $l_b = 24.2$ mm. Dimensionless wall temperatures are 0.467 (800 K), 0.5838 (1000 K) and 0.7006 (1200 K).

elsewhere. The maximum of the Zeldovich flux satisfies

$$\frac{c'}{c} = \frac{\dfrac{c'_e}{c_e} - \dfrac{3\eta T'}{2T}}{1 + 2\epsilon^3\eta^3 T^3} = \frac{1}{1 + 2\epsilon^3 T^3 \left(\ln \dfrac{c}{c_e}\right)^3} \left(\frac{\Lambda}{2\epsilon T} - 1 - \frac{3}{2}\ln\frac{c}{c_e}\right)\frac{T'}{T}, \qquad (3.17)$$

in which we have used (3.8). This is quite close to the maximum of the supersaturation $\eta = \ln(c/c_e)$ whose location satisfies

$$\frac{c'}{c} = \frac{c'_e}{c_e} = \left(\frac{\Lambda}{2\epsilon T} - 1\right)\frac{T'}{T}. \qquad (3.18)$$

Since $\epsilon \ll 1$, both these maxima should be close to the inflection point of c in which c' reaches a maximum. This can be appreciated in figure 2, which shows c', η and J_Z (the Zeldovich flux on the right-hand side of (3.5)) normalized to their respective maxima taken from the solution of (3.1)–(3.13) for a wall temperature of 1000 K. Let $x_M < x_*$ be the common value of these maxima as $\epsilon \to 0$. Nucleation occurs only in a narrow interval about x_M inside the condensation region $0 < x < x_*$. The parameter B is very large which, combined with the shape of the Zeldovich flux, means that the right-hand side of (3.5) behaves as a delta function source term whose role is to create rapidly a basal condensate number density near x_M. Let ρ_b and n_b be
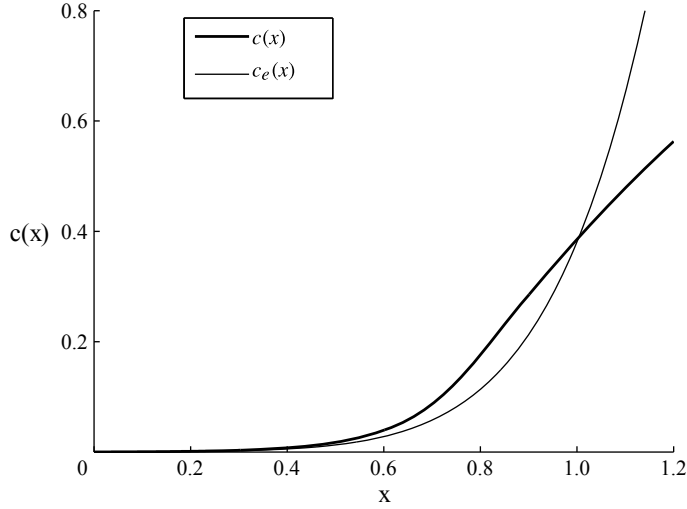
FIGURE 3. $c(x)$ (thick line) and $c_e(x)$ for $\tilde{T}_w = 1000$ K.

reference values for the basal droplet number density and basal number of condensed vapour molecules, respectively (so that $\rho_b n_b$ is the basal condensate number density). Compared to vapour condensation on droplets, little vapour is lost due to nucleation and therefore we can ignore the corresponding term in (3.12). As $B \gg 1$, $c \approx c_e$ except in a narrow condensation layer (which nevertheless includes the even narrower droplet nucleation region) whose length is obtained by balancing c'' and the right-hand side of (3.12). This yields a length

$$\delta = \frac{1}{\sqrt{B\rho_b n_b^{2/3}}} \tag{3.19}$$

which measures the width of the condensation layer in which there is supersaturation and therefore the vapour condenses on the droplets created about x_M. B plays an similar role to the scavenging parameter R in the case of heterogeneous condensation (Neu *et al.* 2009).

The boundary conditions (3.6) and (3.10) can be replaced by the following conditions at the location x_* of the dew point interface Γ:

$$\rho(x_*) = 0, \quad n(x_*) = 0. \tag{3.20}$$

Moreover, at x_* we have

$$c(x_*) = c_e(x_*), \quad c'(x_*-) = c'(x_*+). \tag{3.21}$$

4. Lower and upper bounds for c and x_* and deposition rates

Inside the condensation region $0 < x < x_*$ we have positive supersaturation and $c(x) > c_e(x)$, as shown in figure 3. The maximum possible value of x_* would be reached if $c(x)$ and $c_e(x)$ are tangent at x_*. In such a case, the width of the condensation layer (CL) with positive supersaturation is zero and the vapour density
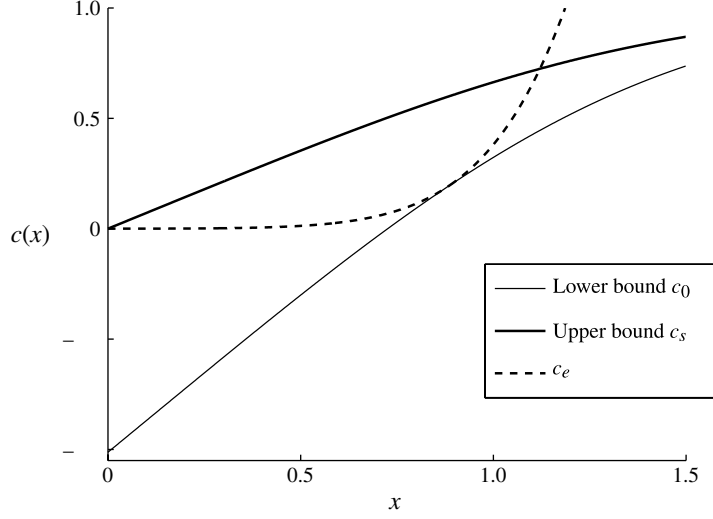
FIGURE 4. Upper and lower bounds for the vapour number density at $\tilde{T}_w = 1000$ K.

profile $c(x)$ reaches its lowest possible value. This profile is the BVP

$$c'' + S_c\, u\, c' = 0, \quad x > 0, \tag{4.1}$$

$$c(x_*) = c_e(x_*), \quad c'(x_*-) = c'(x_*+), \quad c(\infty) = 1. \tag{4.2}$$

The solution of the BVP (4.1)–(4.2) for $x > x_*$ and

$$c(x) = c_e(x), \quad x \leqslant x_*, \tag{4.3}$$

is the 0-CL theory first proposed and studied by Castillo & Rosner (1989) for heterogeneous vapour condensation on solid particles. The solution of (4.1)–(4.2) can be written as (Neu *et al.* 2009)

$$c(x) = 1 + \frac{c_* - 1}{\Psi(x_*)}\Psi(x) \quad \text{where } \Psi \text{ solves} \tag{4.4}$$

$$\Psi'' + S_c\, u\, \Psi' = 0, \quad \Psi(0) = 1, \quad \Psi(\infty) = 0. \tag{4.5}$$

To find x_*, we have to pick a trial value x_T, solve the BVP (4.5) and check whether the following relation, derived from the Clausius–Clapeyron relation (3.8), holds for x_T:

$$c'_e(x) = \left[1 - \frac{\epsilon T(x)}{\Lambda}\right]\frac{\Lambda T'(x)}{\epsilon T(x)^2}\, c_e(x). \tag{4.6}$$

If (4.6) does not hold for x_T, we change this point until it does. The resulting value is the required x_*. The vapour number density and dew point location found by solving the BVP (4.1)–(4.2) will be denoted by $c_0(x)$ and x_{0*}, respectively.

An upper bound for the profile $c(x)$ is found by solving (4.1) with the lowest possible dew point location, $x_* = 0$. Figure 4 compares this upper bound $c_s(x)$ to $c_0(x)$ and $c_e(x)$.

4.1. Deposition at the wall

Vapour directly condenses on the wall by diffusion and droplets of the condensate arrive there thermophoretically. The fluxes of vapour and condensate at the wall are

$$\tilde{J}_v = -D\tilde{c}'(0) = -\frac{D\tilde{c}_\infty}{l_b}c'(0), \tag{4.7}$$

$$\tilde{J}_c = -\tilde{\rho}(0)\tilde{U}(0)\tilde{n}(0) = -\frac{\alpha\nu\tilde{c}_\infty}{l_b}\frac{T'(0)\rho(0)n(0)}{T(0)}, \tag{4.8}$$

respectively, because $\tilde{u}(0) = 0$ and the thermophoretic velocity becomes $\tilde{U} = \alpha\nu\,(\tilde{T}'/\tilde{T})'$ at the wall. Choosing $\nu\tilde{c}_\infty/l_b$ (4.56×10^{12} cm^{-3} for the parameter values in table 1) as the unit of flux, the non-dimensional fluxes are

$$J_v = \frac{c'(0)}{S_c}, \tag{4.9}$$

$$J_c = \alpha\frac{T'(0)\rho(0)n(0)}{T(0)}, \tag{4.10}$$

where we have omitted the minus sign. The total flux of condensate at the wall is

$$J = J_v + J_c = \frac{c'(0)}{S_c} + \rho(0)n(0)U(0). \tag{4.11}$$

4.2. Temperature profile

The temperature profile is a solution of (3.3) and (3.4) given by (Neu *et al.* 2009)

$$T(x) = 1 + (T_w - 1)\Phi(x) \quad \text{where } \Phi \text{ solves} \tag{4.12}$$

$$\Phi'' + P_r u\,\Phi' = 0, \quad \Phi(0) = 1, \quad \Phi(+\infty) = 0. \tag{4.13}$$

4.3. Maximum wall temperature at which there is a CL

As T_w increases, x_* decreases until $x_* = 0$. This marks the absence of a CL of finite width. At the corresponding wall temperature $T_{w,M}$, which is independent of the model we use to describe vapour condensation on droplets, $J_c = 0$. At $T_{w,M}$, $\Phi_* = \Psi_* = 1$ and $T_{w,M}$ solves (Neu *et al.* 2009)

$$\frac{\Phi'(0)}{\Psi'(0)} = \frac{\epsilon T_{w,M}^2}{(1 - T_{w,M})(\Lambda - \epsilon T_{w,M})}\left\{\frac{T_{w,M}}{T_d}\exp\left[\frac{\Lambda}{\epsilon}\left(\frac{1}{T_{w,M}} - \frac{1}{T_d}\right)\right] - 1\right\}. \tag{4.14}$$

For $T_d = 0.817\,(1400$ K$)$ and $\epsilon/\Lambda = 0.0515$ (as in table 2), we obtain $T_{w,M} = 0.755\,(1293$ K$)$. For $T_{w,M} \leqslant T_w < T_d$ there is no CL, $x_* = 0$, and we have $J_c = 0$. Making use of (4.4) and (4.5) with $\Psi_* = \Psi(0) = 1$, we get the following formula for the deposition at the wall:

$$J = J_v = \frac{[1 - c_e(T_w)]\Psi'(0)}{S_c}. \tag{4.15}$$

5. Numerical results

The BVP (3.3)–(3.13) is ill-conditioned. To solve it and obtain the c, n and ρ profiles, we first find the location of the dew surface, x_*, using the shooting method. In the condensation region, $0 \leqslant x \leqslant x_*$, the BVP is solved by finite differences using a relaxation method with a fairly small time step. We have solved the BVP for wall
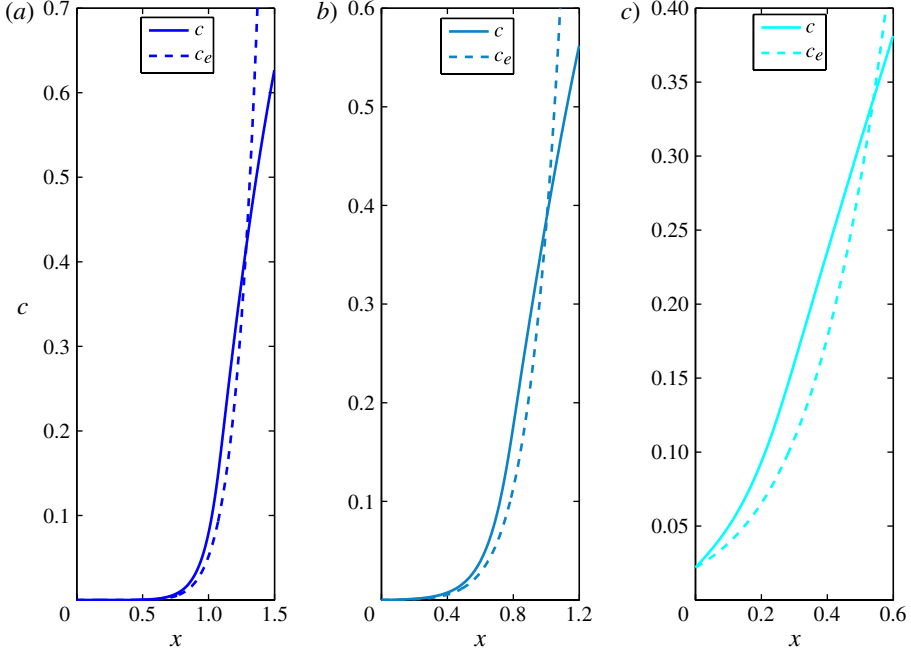
FIGURE 5. (Colour online) Profiles of the vapour number density $c(x)$ at three wall temperatures: (*a*) $\tilde{T}_w = 800$ K, (*b*) $\tilde{T}_w = 1000$ K, (*c*) $\tilde{T}_w = 1200$ K. The intersection between $c(x)$ (solid line) and the Clausius–Clapeyron equilibrium curve marks the location of the dew surface.

temperatures $\tilde{T}_w$ ranging from 800 to 1200 K. For lower $\tilde{T}_w$, compressibility effects of the carrier gas not contemplated in our thermophysical model are important (Filippov 2003). For higher $\tilde{T}_w$, the condensation layer disappears.

The profiles of the vapour and droplet number density profiles are depicted in figures 5 and 6, respectively. Figure 7 depicts the number of condensate molecules $n(x)$. Figure 5 shows that the location of the dew surface approaches the wall as the wall temperature increases, as expected. Figure 6 shows that the droplet density increases as the wall temperature decreases and that an appreciable number of droplets appears for $x < x_*$. Although there are fewer droplets at higher wall temperature, figure 7 shows that they are larger, as the number of condensate molecules carried by them increases with $\tilde{T}_w$.

Figure 8 depicts the consumption of vapour in (3.12) due to condensation on previously nucleated droplets. This is much more important than vapour consumption due to homogeneous nucleation of droplets. We observe how vapour scavenging by droplets changes with the wall temperature. For low $\tilde{T}_w$, nucleation is very active and the droplet density is very large, but the droplet size is small. Nevertheless the net consumption of molecules to form and enlarge droplets is higher than that for larger $\tilde{T}_w$. Figure 9 depicts the profile of the condensation number density. Deposition at the wall is almost constant for low wall temperature and, for each $\tilde{T}_w$, $\rho n = 1$ occurs at a point very close to the inflection point of $c(x)$ all the curves. In turn, this point is very close to x_M where the Zeldovich flux is at a maximum. Droplets are created at a narrow region centred at x_M. According to (3.17), x_M depends strongly on the vapour
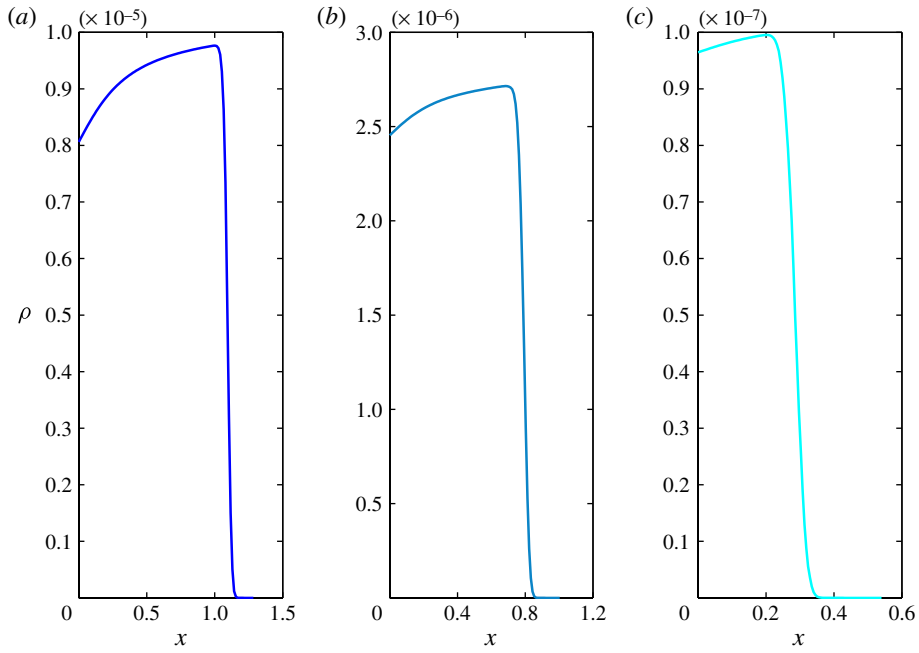
FIGURE 6. (Colour online) Profiles of the droplet number density $\rho(x)$ at three wall temperatures: (a) $\tilde{T}_w = 800$ K, (b) $\tilde{T}_w = 1000$ K, (c) $\tilde{T}_w = 1200$ K.
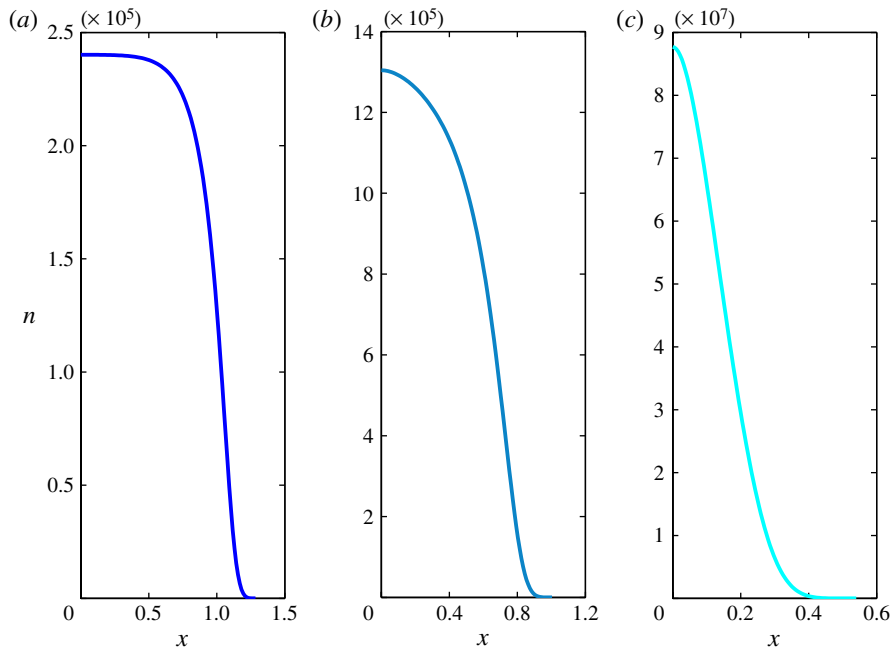

FIGURE 7. (Colour online) Profiles of the condensate number $n(x)$ at three wall temperatures: (a) $\tilde{T}_w = 800$ K, (b) $\tilde{T}_w = 1000$ K, (c) $\tilde{T}_w = 1200$ K.
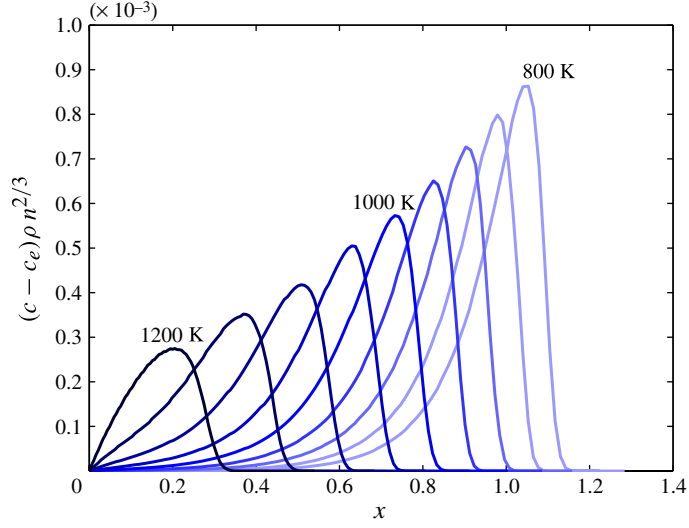
14

FIGURE 8. (Colour online) The function $(c - c_e)\rho\, n^{2/3}$ versus x for wall temperatures: $\tilde{T}_w = 800 + 50j$ K, with $j = 0, 1, \ldots, 8$.
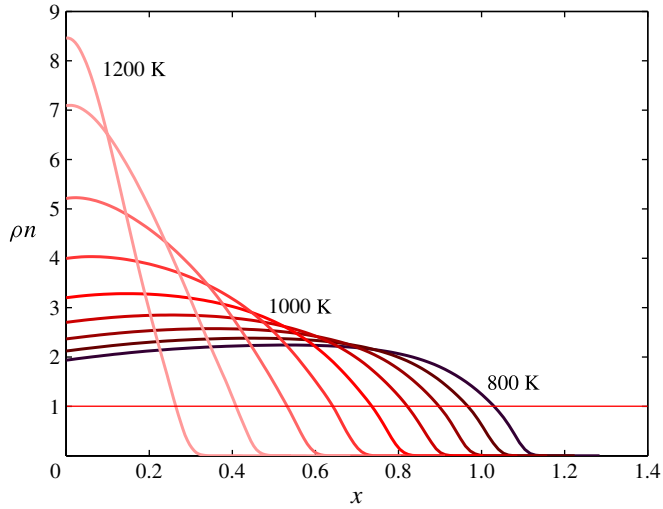
FIGURE 9. (Colour online) Condensate number density ρn versus x for wall temperatures: $\tilde{T}_w = 800 + 50j$ K, with $j = 0, 1, \ldots, 8$.

density profile which, in turn, depends on the droplet density. The latter varies abruptly about x_M.

Figure 10 depicts the deposition rates (4.9)–(4.11) for different T_w. We observe that the deposition rate J_v due to direct condensation of vapour on the wall increases with T_w whereas the deposition rate J_c due to vapour condensation on droplets reaches a minimum at $T_w = 0.55$. In contrast with heterogeneous condensation (see figure 7 of Neu *et al.* 2009), the deposition rate shown in figure 10 is almost constant, except
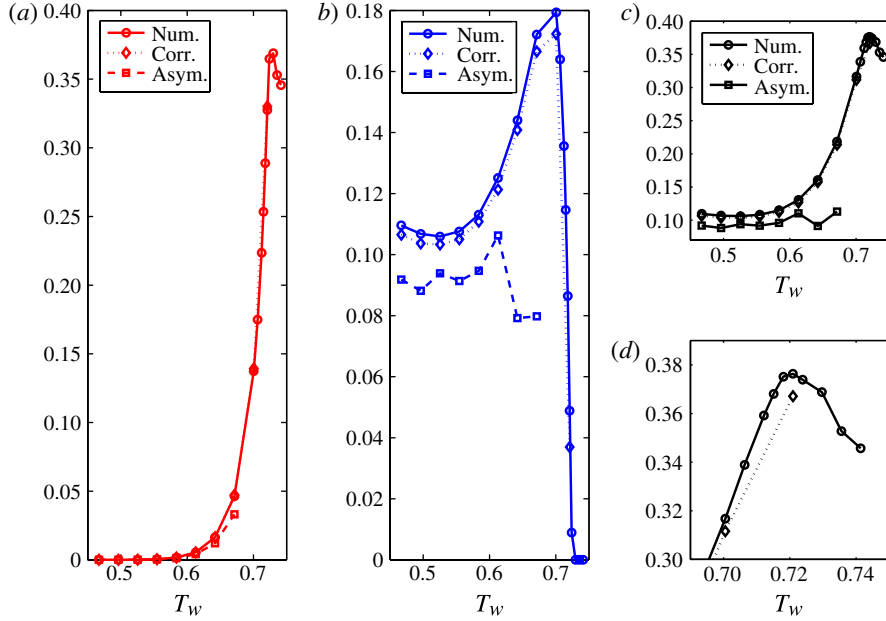
FIGURE 10. (Colour online) Deposition rates (*a*) J_v, (*b*) J_c and (*c*) $J = J_c + J_v$ versus wall temperature. (*d*) shows the total deposition rate J for an interval of T_w about the value at which J has a maximum. The deposition rates obtained by a direct numerical solution of the complete model is compared to approximations found by matched asymptotic expansions (labelled 'Asym.') and by the corrected asymptotic theory of §6.4 (labelled 'Corr.').

at high T_w close to that at which the condensation layer disappears. For low T_w, the nucleation process is very active and the droplet density is very large, but the droplet size is small. The net consumption of vapour molecules to form and enlarge droplets is higher for low T_w. At higher wall temperatures, there are fewer nucleated droplets but their size is higher. In the case of heterogeneous condensation, the number of suspended solid particles that act as condensation sites is constant and they scavenge more vapour as T_w increases. Then the corresponding deposition rate increases with T_w except when the latter is very close to the temperature at which the vapour condenses only on the wall and no longer on the particles.

6. A singular perturbation approach

As explained in §3, droplets are created only in a very narrow nucleation region centred about x_M (where the Zeldovich flux is at a maximum) although the condensation region is wide, comprising the interval from the wall to the nucleation region. Let δ_M be the width of the nucleation region. For x on the interval $x_M + \delta_M/2 < x < x_*$ ending in the dew point x_*, the vapour could condense on droplets but there are none. For $0 < x < x_M - \delta_M/2$, the vapour condenses on the existing droplets but no new droplets are formed. Even when we ignore the contribution of droplet nucleation on the right-hand side of (3.12), locating x_M strongly depends on the vapour density profile which, in turn, is strongly affected by the droplet density. Thus the problem of finding an approximate theory of homogeneous condensation is much more complex than that of heterogeneous condensation in which the droplet number density equals the number density of solid particles. For

16

heterogeneous condensation, approximating the temperature and velocity fields by constant values throughout the narrow CL gave very good results. In the present case, (3.18) for the maximum of the supersaturation already shows that the variation of the temperature profile has to be taken into account. In this section, we propose an asymptotic theory based upon a trial vapour density which interpolates between the upper and lower profiles $c_0(x)$ and $c_s(x)$ of § 4.

6.1. Droplet density profile for a given $c(x)$

Let us rewrite the BVPs posed by (3.5)–(3.6), (3.9)–(3.10) and (3.12)–(3.13) respectively, as

$$\rho' + \alpha \left(\frac{T'}{T}\right)' \frac{\rho}{U} = -\frac{Bc^2}{S_c U \sqrt{2\pi\epsilon}} \exp\left(-\frac{1}{2\epsilon^3 \eta^2 T^3}\right), \tag{6.1}$$

$$C'' + S_c u\, C' + c_e'' + S_c u\, c_e' = B\, C\rho T^{1/2} n^{2/3}, \tag{6.2}$$

$$n' = -\frac{B}{S_c} \frac{C\, T^{1/2} n^{2/3}}{U}, \tag{6.3}$$

where we have ignored the loss of vapour used to form droplets in (3.12) because it is very small compared to the other term. According to (3.20), $\rho = n = 0$ at $x = x_*$ far from the nucleation layer. The vapour number density satisfies $c(+\infty) = 1$, $c(0) = c_e(0)$ and (3.21) at $x = x_*$.

Provided c is known, we can solve (6.1) by the method of matched asymptotic expansions. Let $x_M < x_*$ be the location of the global maximum of the right-hand side of (6.1). The latter is zero except in a narrow layer about x_M, so we can replace (6.1) by

$$\rho_{in}' \sim -\frac{B\, c_M^2}{S_c U_M \sqrt{2\pi\epsilon}} \exp\left(-\frac{1}{2\epsilon^3 \eta_M^2 T_M^3}\right) \exp\left(-\frac{|\beta_M|}{2\epsilon^3 \eta_M^3 T_M^3}(x - x_M)^2\right), \tag{6.4}$$

$$\beta = \frac{\partial}{\partial x}\left[\frac{c'}{c} - \frac{c_e'}{c_e} + \frac{3\eta T'}{2T} + \epsilon^3 \eta^3 T^3 \left(\frac{2c'}{c} - \frac{U'}{U}\right)\right], \tag{6.5}$$

in the immediate neighbourhood of x_M. Here ρ_{in} is the inner approximation to $\rho(x)$ and the subscripts M indicate that the corresponding functions are calculated at x_M. The solution of (6.4) that equals ρ_M at $x = x_M$ and tends to zero as $(x - x_M) \to +\infty$ is

$$\rho_{in}(x) \sim \rho_M \operatorname{erfc}\left(\left|\frac{\beta_M}{2\epsilon^3 \eta_M^3 T_M^3}\right|^{1/2}(x - x_M)\right), \tag{6.6}$$

$$\rho_M = \frac{\epsilon B\, T_M^{3/2} \eta_M^{3/2} c_M^2}{2 S_c U_M |\beta_M|^{1/2}} \exp\left(-\frac{1}{2\epsilon^3 \eta_M^2 T_M^3}\right). \tag{6.7}$$

The outer approximation to $\rho(x)$ obeys (6.1) with zero right-hand side,

$$\rho_{out}' + \alpha\left(\frac{T'}{T}\right)' \frac{\rho_{out}}{U} = 0, \tag{6.8}$$

and the composite solution that approximates $\rho(x)$ uniformly in x is

$$\rho(x) = 2\rho_M \left\{ \exp\left[\alpha \int_x^{x_M} \left(\frac{T'}{T} \right)' \frac{dx}{U} \right] - 1 \right\} H(x_M - x)$$

$$+ \rho_M \, \text{erfc}\left(\left| \frac{\beta_M}{2\epsilon^3 \eta_M^3 T_M^3} \right|^{1/2} (x - x_M) \right). \tag{6.9}$$

6.2. *Trial vapour number density $\gamma(x)$*

In §4 we found that the vapour number density lies between two limit curves $c_0(x)$ and $c_s(x)$ given by solving (4.1) with boundary conditions (4.2) and with $c(0) = c_e(0)$, $c(+\infty) = 1$, respectively. Our trial vapour number density is

$$\gamma_j(x) = c_0 + (c_s - c_0)\frac{j}{N_1}, \quad j = 0, 1, \ldots, N, \tag{6.10}$$

where N is an integer number. Out of these trial functions, we want to extract the best $\gamma_j(x)$, proceeding as follows. Firstly, we calculate the location of the maximum of the Zeldovich flux from the right-hand side of (6.1) with $c(x) = \gamma_j(x)$. This yields points x_{Mj}, $j = 0, 1, \ldots, N$. Similarly, we can calculate the dew point locations x_{*j} where $\gamma_j(x) = c_e(x)$. We now solve (6.3) for $C(x) = \gamma_j(x) - c_e(x)$ with the boundary condition $n(x_{*j}) = 0$:

$$n_j(x) = \left(\frac{B}{3S_c} \int_x^{x_{*j}} \frac{\gamma_j - c_e}{U} T^{1/2} \, dx \right)^3. \tag{6.11}$$

The maximum value of n_j is reached at the wall, $n_j(0)$. Let $\rho_j(x)$ and $2\rho_{Mj}$ be the droplet density (6.9) and its maximum value (6.7) calculated using the trial vapour density $\gamma_j(x)$. We choose as the optimum value of j the one that makes the product $2\rho_{Mj}n_j(0)$ (maximum condensate number density) closest to $c_\infty = 1$ (maximum vapour density). We shall denote by J this optimum value of j. Figure 11 compares $\rho_J(x)$ to the droplet density obtained by numerically solving the whole problem for three different wall temperatures. We see that the agreement is fairly good and it improves as the wall temperature decreases. At higher temperatures, the method that we use to calculate $\rho_J(x)$ breaks down (e.g. at 1200 K).

6.3. *Approximation for $n(x)$ and $c(x)$ in the condensation region*

The optimal $\gamma_J(x)$ and $n_J(x)$ are reasonable approximations in the dry region $x > x_{MJ}$, but we need to improve them in the nucleation–condensation region $0 < x < x_{MJ}$. We solve (6.2)–(6.3) using the composite droplet density $\rho_J(x)$ and the approximate location x_{MJ}. The boundary conditions at x_{MJ} will be given there by the values of $\gamma_J(x)$ and $n_J(x)$, to which $c(0) = c_e(0)$ is to be added. From (6.3), we obtain

$$C = -\frac{3S_c}{B} \frac{U}{T^{1/2}} Y', \quad Y = n^{1/3}. \tag{6.12}$$

Inserting this in (6.2), we get the third-order equation

$$Y''' + \left(\frac{2U'}{U} - \frac{T'}{T} + S_c u \right) Y'' + \left[\frac{\sqrt{T}}{U} \left(\frac{U}{T^{1/2}} \right)' + S_c \left(\frac{uU'}{U} - \frac{uT'}{2T} \right) - B\rho_J\sqrt{T}Y^2 \right] Y'$$

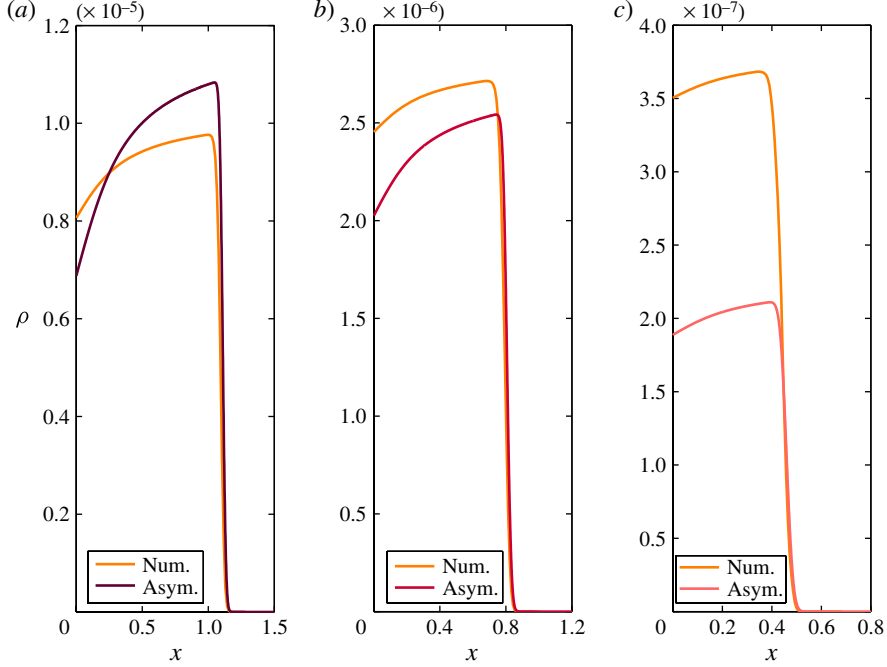$$= \frac{B\sqrt{T}}{3S_c U} (c_e'' + S_c u c_e'), \tag{6.13}$$

FIGURE 11. (Colour online) Numerically obtained and approximate droplet density profiles, $\rho(x)$ (labelled 'Num.') and $\rho_J(x)$ (labelled 'Asym.') at wall temperatures of (a) 800 K, (b) 1000 K, (c) 1150 K.

to be solved with the boundary conditions

$$Y'(0) = 0, \quad Y'(x_{MJ}) = -\frac{B}{3S_c}\frac{T^{1/2}}{U}(\gamma_J - c_e)\bigg|_{x_{MJ}}, \quad Y(x_{MJ}) = [n_J(x_{MJ})]^{1/3}. \quad (6.14)$$

There is a narrow boundary layer near x_{MJ} in which Y satisfies the boundary conditions (6.14) and increases rapidly to some constant value. Rescaling x as $X = (x - x_{MJ})/\mu_x$ and assuming that $c_e'' = O(1)$, we find the scales of x, C and n from (6.2) and (6.3):

$$\mu_x = B^{-3/8}\rho_{MJ}^{-1/8}\delta_e^{1/4}, \quad \mu_C = B^{-3/4}\rho_{MJ}^{-1/4}\delta_e^{-1/2}, \quad \mu_n = B^{-3/8}\rho_{MJ}^{-9/8}\delta_e^{-3/4}. \quad (6.15)$$

For typical values of $B \approx 10^4$, $\rho_{MJ} \approx 10^{-6}$, $\delta_e \approx 0.16$, we get $\mu_x \approx 0.112$, $\mu_C \approx 0.08$, $\mu_n^{1/3} \approx 55.28$. Thus we may assume $\mu_C \ll \mu_x \ll 1 \ll \mu_n$ and $\mu_x = O(\delta_e)$. We now rescale $\rho = \rho_{MJ}r \approx \rho_{MJ}H(-X)$ (assuming a negligible width of the Zeldovich peak, $|2\epsilon^3\eta_{MJ}^2 T_{MJ}^3/\beta_{MJ}|^{1/2} \ll \mu_x$), $Y = \mu_n^{1/3}y$, $X = (x - x_{MJ})/\mu_x$ and keep leading-order terms in (6.13). The resulting equation and rescaled boundary conditions (6.14) are

$$\frac{\partial^3 y}{\partial X^3} - 2T_{MJ}^{1/2}y^2\frac{\partial y}{\partial X} = \frac{\sqrt{T_{MJ}}}{3S_c U_{MJ}}\delta_e(c_e'' + S_c u_{MJ}c_e'), \quad X < 0, \quad (6.16)$$

$$\left.\begin{array}{l} y(0) = B^{1/8}\rho_{MJ}^{3/8}\delta_e^{1/4}[n_J(x_{MJ})]^{1/3}, \quad \dfrac{\partial y}{\partial X}(0) = -\dfrac{\sqrt{T_{MJ}}}{3S_c U_{MJ}}\dfrac{\gamma_J(x_{MJ}) - c_e(x_{MJ})}{\mu_C}, \\[2mm] \dfrac{\partial y}{\partial X}\left(-\dfrac{x_{MJ}}{\mu_x}\right) = 0. \end{array}\right\} \quad (6.17)$$

19

The BVP (6.16)–(6.17) has a unique solution that produces $y(-x_{MJ}/\mu_x) = y_w$, from which $n_w = B^{-3/8}\rho_{MJ}^{-9/8}\delta_e^{-3/4}y_w^3$ is an unscaled number of condensate molecules at the wall, $X_w = -x_{MJ}/\mu_x$ $(x_{MJ} \gg \mu_x)$.

The boundary layer solution fixes ρ_J as the inner solution (6.6), thereby underestimating $n = Y^3$. y has an inflection point at $X = X_n$ and $\partial^2 y/\partial X^2$ and $\partial^3 y/\partial X^3$ become small for $X < X_n$. To correct this approximation to the solution of (6.13)–(6.14), we add to it a solution of the outer problem:

$$n' = -\frac{c_e'' + S_c u c_e'}{S_c \rho_J U}, \quad 0 < x < x_n \equiv x_{MJ} - \mu_x X_n, \tag{6.18}$$

$$n(x_n) = 0. \tag{6.19}$$

Equation (6.18) follows from (6.13) if, on the left-hand side of the former equation, we ignore all terms except the last one and use $n = Y^3$ in the result. Thus the number of condensate molecules for $x < x_{MJ}$ is $n \approx n_0(x)$,

$$n_0 = \frac{H(x_n - x)}{S_c} \int_x^{x_n} \frac{c_e'' + S_c u c_e'}{\rho_J U} \, \mathrm{d}x + \mu_n \left[y\left(\frac{x - x_{MJ}}{\mu_x}\right) \right]^3, \tag{6.20}$$

where the second term is the inner solution. The corresponding $C = c - c_e$, which we shall call $C_0(x)$, is given by (6.12) but it does not satisfy $C(0) = 0$. The correction is given by a boundary layer problem in which only C'' and the right-hand side of (6.2) are kept. Its solution is

$$C_{0,B.L.}(x) = C_0(0) \left[1 - \exp\left(-x\sqrt{B\rho(0)T_w^{1/2} [n_0(0)]^{2/3}} \right) \right], \tag{6.21}$$

and the corresponding composite approximation becomes

$$C_{unif}(x) = C_0(x) - C_0(0) \exp\left(-x\sqrt{B\rho(0)T_w^{1/2} [n_0(0)]^{2/3}} \right). \tag{6.22}$$

The vapour density profile is compared to the asymptotic solution in figure 12. As in the case of the droplet density profile (figure 11), the asymptotic theory approximates the vapour number density better than the number of condensate molecules shown in figure 13.

6.4. *Corrected profiles for higher wall temperature*

The asymptotic theory described above is an acceptable approximation except when $\tilde{T}_w$ becomes larger and the width of the boundary layer decreases. Two shortcomings of the asymptotic theory come to the fore. Firstly, the calculation of the maximum Zeldovich flux breaks down and we cannot find the optimal vapour profile $\gamma_J(x)$. Secondly, we cannot neglect $\partial^2 y/\partial X^2$ and $\partial y/\partial X$ in (6.13) when $\tilde{T}_w \geqslant 1000$ K. For $\tilde{T}_w$ close to 1200 K there is no boundary layer solution for n and C, although there is still one for ρ. As a result, the values of ρ and n at the wall differ appreciably from those given by the numerical solution of the thermophysical model.

We have developed a corrected asymptotic theory by improving the optimal trial vapour density and solving the complete third-order equation (6.13). We need to take into account that the maxima for c', η and J_z are not coincident: see figure 2. In the corrected theory, we obtain x_M graphically by solving the functional equation $\rho_{M1}(j, k) - \rho_{M2}(j, k) = 0$, whose terms are depicted in figure 14. Here $\rho_{M1}(j, k)$ is the maximum value of the droplet density profile found from (6.1) with, $x_{Mk} = x_{*0}k/N$,
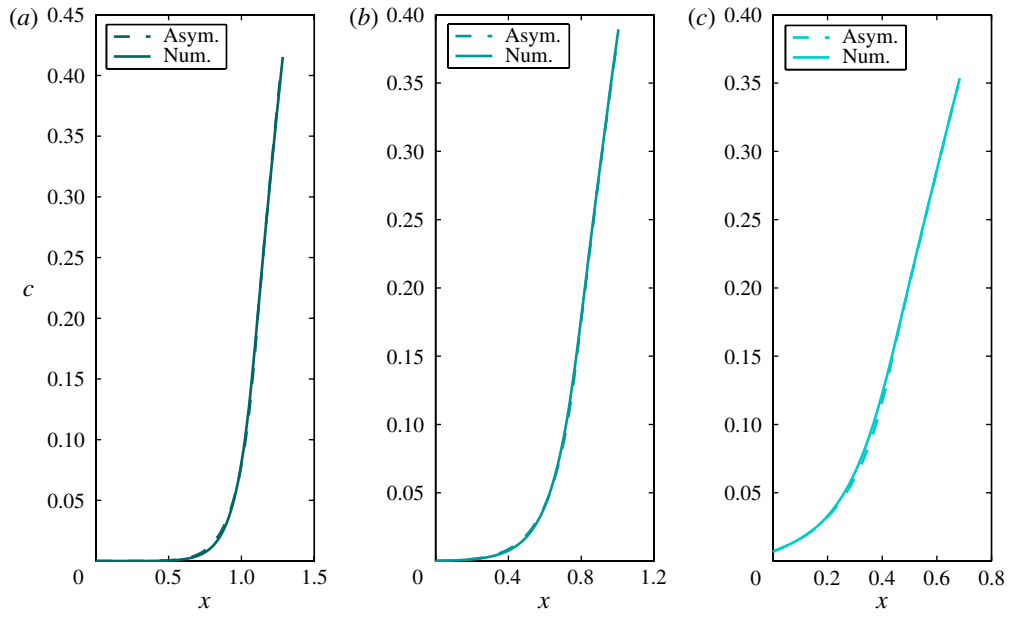
FIGURE 12. Numerically and asymptotically obtained vapour density profiles at wall temperatures of (*a*) 800 K, (*b*) 1000 K, (*c*) 1150 K.
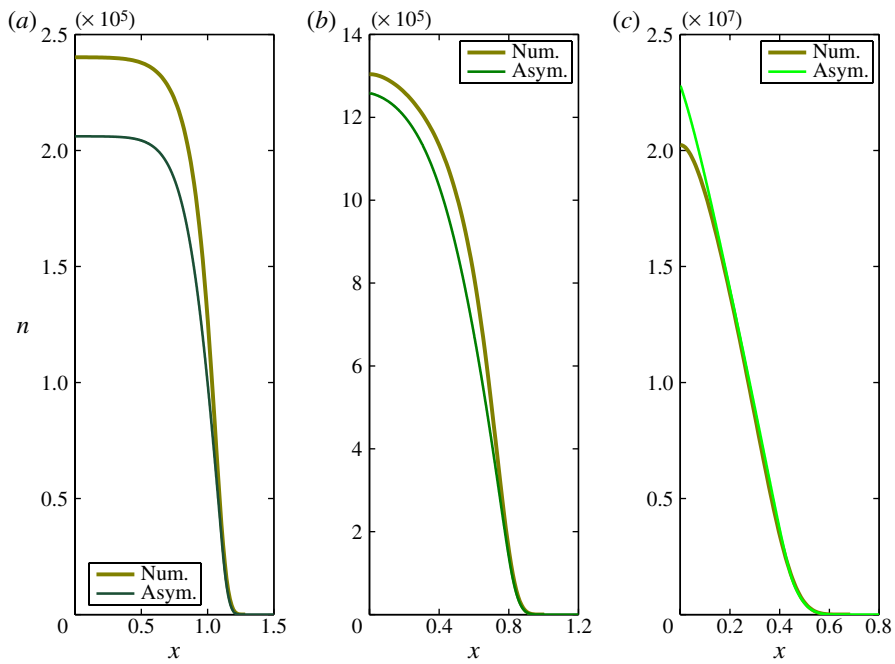

FIGURE 13. (Colour online) Numerically obtained and approximate number of condensate molecules, $n(x)$ at wall temperatures of (*a*) 800 K, (*b*) 1000 K, (*c*) 1150 K.
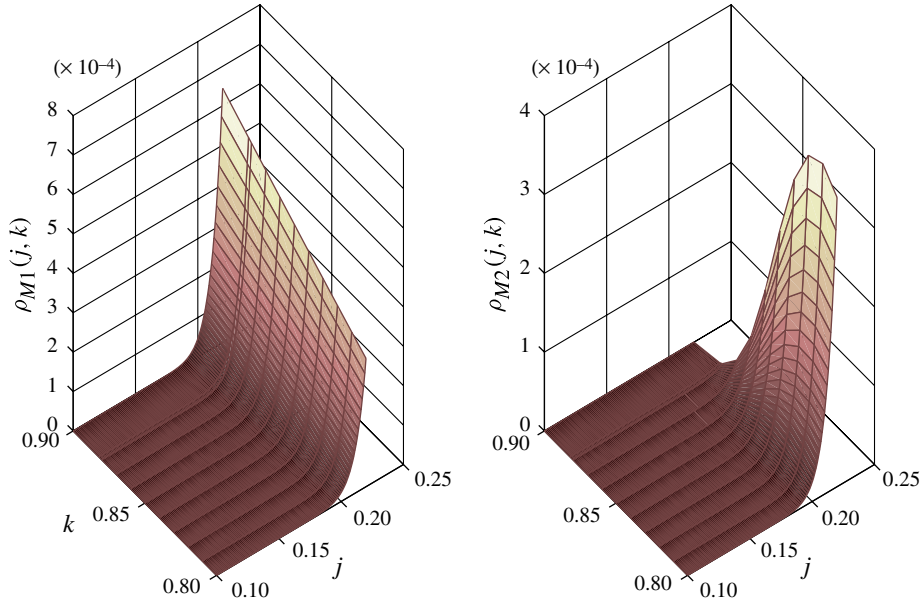
FIGURE 14. (Colour online) Functions $\rho_{M1}(j, k)$ and $\rho_{M2}(j, k)$ for $T_w = 1000$ K. $\rho_{MK}(j)$ is the intersection curve of both surfaces.
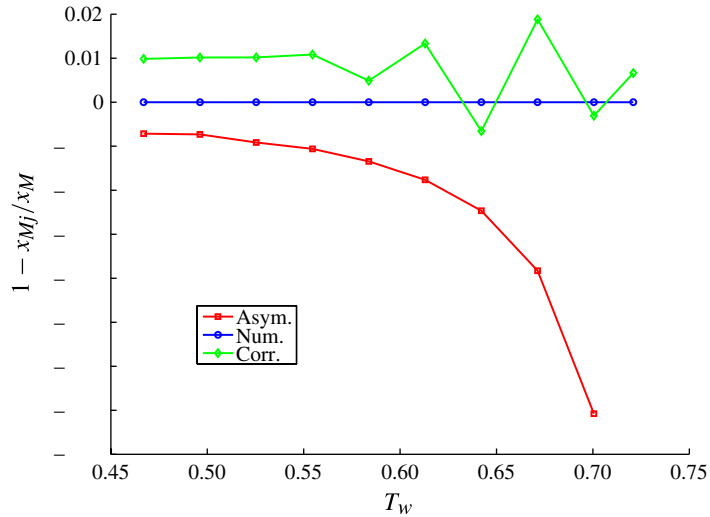

FIGURE 15. (Colour online) Estimated location x_{MJ} at which the Zeldovich droplet nucleation rate is at a maximum compared to the numerically obtained value x_M as a function of the wall temperature T_w.

$k = 0, 1, \ldots, N$, and x_{*0} given by the 0-CL theory, and $\rho_{M2}(j, k)$ is the maximum value of the droplet density profile given by the composite solution (6.9) with $x_M = x_{Mk}$ and $c(x) = \gamma_j(x)$.

Figure 15 compares the location of the point at which the Zeldovich droplet nucleation rate is at a maximum as given by the asymptotic theory of previous
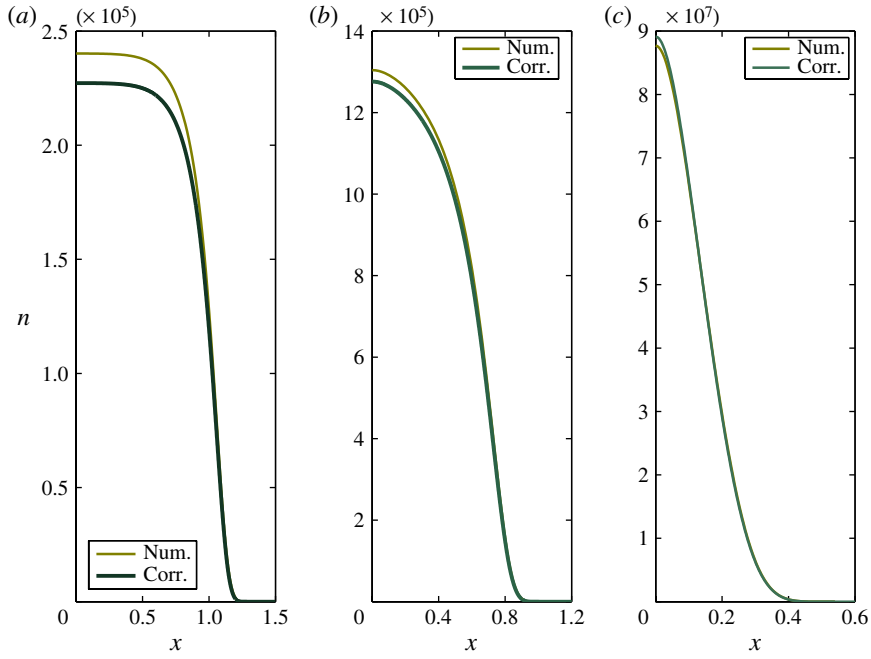
FIGURE 16. (Colour online) Corrected and numerical condensate number profiles for wall temperatures of (*a*) 800 K, (*b*) 1000 K, (*c*) 1200 K.

subsections, by the corrected theory and by numerical solution of the complete model equations. The earlier asymptotic theory performs poorly for higher T_w (and it gives no solution for $T_w > 0.7$) whereas the corrected theory still works for the whole range of T_w. Figures 16 and 17 compare the corrected asymptotic theory and the numerical solution of the whole problem. In both cases, the corrected theory greatly improves the results of the earlier asymptotic theory. We have not shown the vapour number density profile given by the corrected asymptotic theory as it coincides within 1 % relative error with that of the numerical solution of the whole problem. Both curves would overlap if depicted together. The deposition rates depicted in figure 10 are reasonably given by our earlier asymptotic theory except for fairly high T_w, for which this approximation breaks down. The corrected asymptotic theory gives quite accurate approximations for the deposition rates even at high T_w close to the maximum deposition rate.

7. Conclusions

We have considered homogeneous condensation of vapours mixed with a carrier gas in the stagnation point boundary layer flow near a cold wall. Droplets are homogeneously nucleated at the Zeldovich rate in a very narrow region and their size increases from the negligible size of the critical nucleus as they move towards the wall by thermophoresis. The mean free path is much larger than the droplet size and therefore the nucleated droplets capture vapour according to free-molecular-regime law. In our thermophysical model, we have ignored the Soret and Dufour effects and have assumed that the heat of vapourization is much larger than the Boltzmann constant times the temperature far from the wall. The carrier gas is assumed to
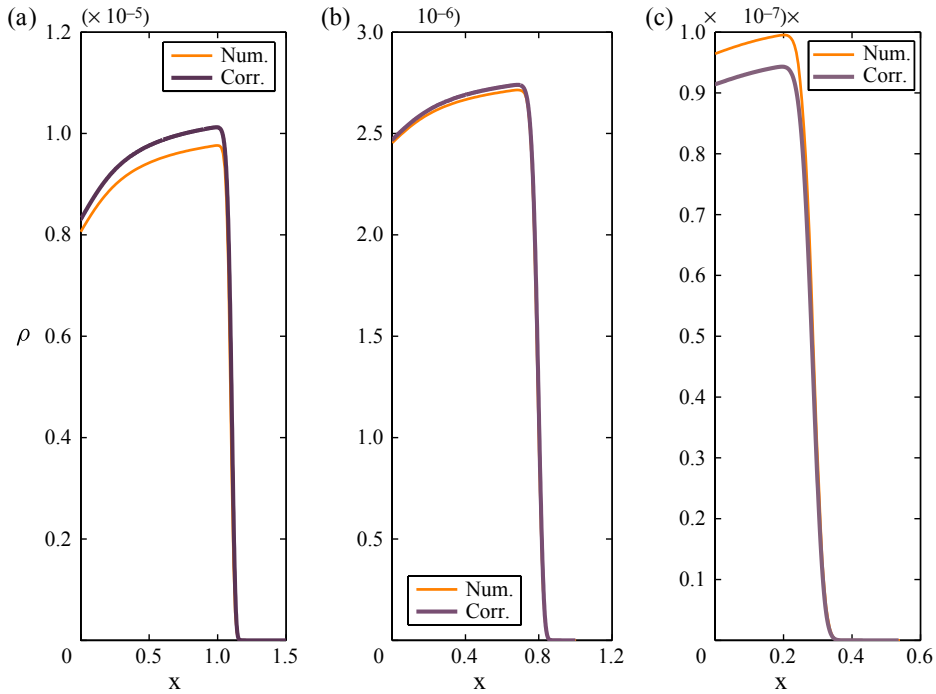
FIGURE 17. (Colour online) Corrected and numerical droplet number density profiles for wall temperatures of (*a*) 800 K, (*b*) 1000 K, (*c*) 1200 K.

be incompressible for the range of wall temperatures that we consider. Under these conditions, vapour condensation occurs in a condensation layer whose distance to the wall, width and characteristics depend on the parameters of the problem.

We have presented an asymptotic theory of the homogeneous condensation process, calculated the profiles of vapour density, droplet density and number of condensate molecules, and the deposition rates at the wall, and compared them to direct numerical simulation of the equations governing the model. Elaborating a theory of homogeneous condensation is more complex than in the case of heterogeneous condensation, where the number of droplets coincides with that of solid particles suspended in the gas. In the case of homogeneous condensation, the droplet density is higher than the equilibrium vapour density (the 0-CL theory in Neu *et al.* 2009) and lower than the vapour density profile in the absence of condensation. We select a trial vapour density which interpolates between these two bounds and satisfies the condition that the maximum number density of the condensate be close to the maximum vapour number density. We then calculate the corresponding droplet density profile using that droplets nucleate in a very narrow region about the peak of the Zeldovich rate. With this profile, we solve the equations for the condensate number of molecules and the vapour density by matched asymptotic expansions. This process is iterated using the new vapour density until a reasonable convergence is reached. For large wall temperatures, the calculation of the maximum Zeldovich rate breaks down and we corrected our asymptotic procedure by selecting the optimal trial vapour density in a different way: we interpolate between vapour density profiles and locations of the dew surface. We also need to correct the equations in the condensation layer which is now very close to the wall. Our theory approximates the vapour number density very well and gives

good approximations to the droplet density, the number of condensate molecules and the deposition rate.

We can extend our theory in several directions of interest in engineering, while keeping the paramount simplification that the condensable vapour is very diluted, and therefore the velocity and temperature fields are independent from nucleation–condensation processes. Firstly, we can consider self-similar boundary layer flows, such as wedge flows (García Ybarra & Castillo 1997; Schlichting & Gersten 2000), that are more general than the stagnation point flow. In an appropriate mass coordinate, the velocity field is described by a modified Falkner–Skan equation and the rest of the calculation is straightforward along the lines of the present paper. Secondly, we can consider the case of a compressible carrier gas with temperature-dependent viscosity (Filippov 2003). In this case, the equations for the temperature and velocity are coupled but their profiles are self-similar in the appropriate mass coordinate (Filippov 2003). Our methods can be applied to solve this more complete thermophysical model. Yet another scenario important for aerosols (Davis 1983; Jacobson 1996; Friedlander 2000) and climate applications (Pruppacher & Klett 1997) is to consider what happens when a flow of air carrying supersaturated water vapour encounters a quiescent cold gas and condensation occurs. The resulting boundary layer flow should be similar to the case considered in this paper except for different boundary conditions at the 'wall' formed by the quiescent cold gas. In many applications, it is important to use nucleation rates that give a better description of experimental conditions than the Zeldovich rate we use here. Three such rates are discussed by Sinha *et al.* (2009) and references they cite. See also Nowakowski & Ruckenstein (1991) for deviations from the classical nucleation rate at small sizes of the critical nucleus. Other improvements refer to the droplet growth law when the droplets are comparable to or larger than the mean free path (Sinha *et al.* 2009). Our calculations can be repeated for these other nucleation and growth laws with the appropriate modifications.

Acknowledgements

REFERENCES

CASTILLO, J. L. & ROSNER, D. E. 1988 A nonequilibrium theory of surface deposition from particle-laden, dilute condensible vapour-containing laminar boundary layers. *Intl J. Multiphase Flow* **14**, 99–120.

CASTILLO, J. L. & ROSNER, D. E. 1989 Theory of surface deposition from a unary dilute vapour-containing steam, allowing for condensation within the laminar boundary layer. *Chem. Engng Sci.* **44**, 925–937.

DAVIS, E. J. 1983 Transport phenomena with single aerosol particles. *Aerosol Sci. Technol.* **2**, 121–144.

DELALE, C. F. & CRIGHTON, D. G. 1998 Prandtl–Meyer flows with homogeneous condensation. Part 1. Subcritical flows. *J. Fluid Mech.* **359**, 23–47.

FILIPPOV, A. V. 2003 Simultaneous particle and vapour deposition in a laminar boundary layer. *J. Colloid Interface Sci.* **257**, 2–12.

FRIEDLANDER, S. K. 2000 Smoke, dust and haze. In *Fundamentals of Aerosol Dynamics*, 2nd edn. Oxford University Press.

GARCÍA YBARRA, P. L. & CASTILLO, J. L. 1997 Mass transfer dominated by thermal diffusion in laminar boundary layers. *J. Fluid Mech.* **336**, 379–409.

GÖKOGLU, S. A. & ROSNER, D. E. 1986 Thermophoretically augmented mass transfer rates to solid walls across laminar boundary layers. *AIAA J.* **24**, 172–179.

JACOBSON, M. Z. 1996 Development and application of a new air pollution modelling system. Part 1. *Atmos. Environ.* **30**, 1939–1963.

LUO, X. S., LAMANNA, G., HOLTEN, A. P. C. & VAN DONGEN, M. E. H. 2007 Effects of homogeneous condensation in compressible flows: Ludwieg-tube experiments and simulations. *J. Fluid Mech.* **572**, 339–366.

NEU, J. C., BONILLA, L. L. & CARPIO, A. 2009 Theory of surface deposition from boundary layers containing condensable vapour and particles. *J. Fluid Mech.* **626**, 183–210.

NOWAKOWSKI, B. & RUCKENSTEIN, E. 1991 A kinetic approach to the theory of nucleation in gases. *J. Chem. Phys.* **94**, 1397–1402.

PAOLI, R., HELIE, J. & POINSOT, T. 2004 Contrail formation in aircraft wakes. *J. Fluid Mech.* **502**, 361–373.

PEETERS, P., LUIJTEN, C. C. M. & VAN DONGEN, M. E. H. 2001 Transport phenomena with single aerosol particles. *Intl J. Heat Mass Transfer* **44**, 181–193.

PRUPPACHER, H. R. & KLETT, J. D. 1997 *Microphysics of Clouds and Precipitation*. Kluwer.

PYYKÖNEN, J. & JOKINIEMI, J. 2003 Modelling alkali chloride superheater deposition and its implications. *Fuel Process. Technol.* **80**, 225–262.

ROSNER, D. E. 2000 *Transport Processes in Chemically Reacting Flow Systems*. Dover.

SCHLICHTING, H. & GERSTEN, K. 2000 *Boundary Layer Theory*, 8th edn. Springer.

SINHA, S., WYSLOUZIL, B. E. & WILEMSKI, G. 2009 Modelling of H_2O/D_2O condensation in supersonic nozzles. *Aerosol Sci. Technol.* **43**, 9–24.

TANDON, P. & MURTAGH, M. 2005 Particle–vapour interaction in deposition systems: influence on deposit morphology. *Chem. Engng Sci.* **60**, 1685–1699.

WU, D. T. 1997 Nucleation theory. *Solid State Phys.* **50**, 37–187.

ZHENG, F. 2002 Thermophoresis of spherical and non-spherical particles: a review of theories and experiments. *Adv. Colloid Interface Sci.* **97**, 253–276.